The Astrophysical Journal, 837:22 (8pp), 2017 March 1 https://doi.org/10.3847/1538-4357/aa5da9


# Anomalous Galactic Dynamics by Collusion of Rindler and Cosmological Horizons

Maurice H. P. M. van Putten
Room 614, Astronomy and Space Science, Sejong University, 98 Gunja-Dong Gwangin-gu, Seoul 143-747, Korea; mvp@sejong.ac.kr
*Received 2016 October 14; revised 2017 January 30; accepted 2017 January 30; published 2017 February 28*

## Abstract

In holography, the dimensional reduction of phase space to two dimensions defines a dynamical dark energy of $\Lambda = (1-q)H^2$, associated with the cosmological horizon at a Hubble radius of $R_H = c/H$, and inertia $m$ of baryonic matter at acceleration $\alpha$ in terms of a thermodynamic potential $U = mc^2$ of Rindler horizons at $\xi = c^2/\alpha$. Here, $H$ is the Hubble parameter with deceleration $q$ and $c$ is the velocity of light. In weak gravity, $m$ drops below Newton's value $m_0$ as $\alpha < a_H$, when Rindler horizons fall beyond the cosmological horizon. The onset to weak gravity across $\alpha = a_H$ is sharp by causality. Striking evidence is found in galaxy rotation curves, whose asymptotic dynamics is parameterized by Milgrom's scale of acceleration $a_0 = (cH/2\pi)\sqrt{1-q}$. This onset presents a new challenge for canonical dark matter distributions on galactic scales in ΛCDM. Instead, future galaxy surveys may determine $Q_0 = dq(z)/dz|_{z=0}$, to provide a direct test of dynamical dark energy ($Q_0 > 2.5$) versus ΛCDM ($Q_0 < 1$) and establish a bound of $10^{-30}$ eV on the mass of the putative dark matter particle with clustering limited to galaxy clusters.

*Key words:* cosmological parameters – galaxies: kinematics and dynamics – gravitation

## 1. Introduction

Modern observations show overwhelming evidence for dynamics in galaxies and cosmological evolution, which defies extrapolation of Newtonian gravity and its embedding in classical general relativity. In the cosmic microwave backround in the framework of ΛCDM, reconciliation with the latter is made by invoking volume densities of dark energy and dark matter (Ade et al. 2014). On astrophysical scales, a similar need for dark matter appears in rotation curves of spiral galaxies, notably beyond a few kiloparsecs of the central bulge at accelerations below the cosmological scale

$$a_{dS} = cH, \tag{1}$$

where $c$ denotes the velocity of light and $H$ is the Hubble parameter (Famae & McGaugh 2012). Specifically, accelerations $\alpha \ll a_{dS}$ appear to harden emperically by the baryonic Tully–Fisher inverse distance law (McGaugh 2005, 2011, 2012). This asymptotic regime of weak gravity is equivalent to Milgrom's law (Milgrom 1983; McGaugh & Schombert 2015), distinct from Newtonian's theory in $\alpha > a_{dS}$ based on baryonic matter alone. Recently, the same is identified in elliptical galaxies and dwarf spheroidals, suggesting a universal origin (Lelli et al. 2016; McGaugh & Lelli 2016). Furthermore, the present day value $H_0 \simeq 69\ \mathrm{km\ s^{-1}\ Mpc^{-1}}$ of the Hubble parameter in ΛCDM (Ade et al. 2014) is in persistent tension with $H_0 \simeq 73\ \mathrm{km\ s^{-1}\ Mpc^{-1}}$ measured in low-redshift surveys (Riess et al. 2016).

It is tempting but not imperative to attribute the above to concentrations of dark matter on cosmological and galactic scales. However, the associated scale of acceleration

$$\frac{cH_0}{2\pi} \simeq 1\ \mathrm{\AA\ s^{-2}}, \tag{2}$$

is tiny, some four orders below the scales at which Newtonian mechanics and gravitational attraction have been tested. It may reflect a hitherto unappreciated low-energy scale in the cosmological vacuum that perturbs motion in possibly unfamiliar ways, e.g., Modified Newtonian Dynamics (e.g., Bekenstein 2009), obviating the need for dark matter on galactic scales.

In ΛCDM, the accelerated expansion of the universe currently shows an initial approach to a de Sitter state, driven by a finite density of dark energy (Perlmutter et al. 1999), which is inferred from a deceleration parameter

$$q = \frac{1}{2}\Omega_M - \Omega_\Lambda < 0 \tag{3}$$

with fractions of cold dark matter $\Omega_M$ and dark energy $\Omega_\Lambda$, normalized to closure matter density $\rho_c = 3H_0^2/8\pi G$ with Newton's constant $G$. The conclusion (3) is based on the three-flat Friedmann–Robertson–Walker (FRW) line-element

$$ds^2 = -dt^2 + a(t)^2(dx^2 + dy^2 + dz^2) \tag{4}$$

with a dynamical scale factor $a(t)$, $H_0 = |\dot{a}/a|_{z=0}$, and $q = -\ddot{a}a/\dot{a}^2$ in evolution according to the theory of general relativity, assuming a classical background vacuum with no relevant low-energy scale(s).

General relativity provides a four-covariant embedding of Newton's law of gravitation by a mixed elliptic-hyperbolic system of equations. Hyperbolicity ensures local causality in gravitational wave motion, which was recently detected (LIGO-Virgo Collaboration 2016) and parameterized by the unit of luminosity $L_0 = c^5/G$. The elliptic part carries causality in a cosmological horizon at a Hubble radius of $R_H = c/H_0$ in (4). Classically, galactic dynamics appears disconnected from the cosmological background, by the huge discrepancy between galactic scales and $R_H$.

The t Hooft *Ansatz* of holography posits a dimensional reduction of phase space of spacetime in matter and fields to surface area of an enclosing surface (Bekenstein 1981; t Hooft 1993; Susskind 1995). In astrophysics and cosmology, holography at finite vacuum temperature seen by accelerating observers has potentially radical implications for our interpretation of dark energy and dark matter. Upon conversion to geometrical units with $c = G = 1$, a surface density of

$[\sqrt{\Lambda}] = \mathrm{cm}^{-1}$ is obtained from a dark energy volume density $\Lambda$, $[\Lambda] = \mathrm{cm}^{-2}$. Thus, $\sqrt{\Lambda}$ opens a window to perturb gravitation on galactic scales associated with $\Lambda$ relevant to cosmological evolution. Thermodynamic properties of the cosmological horizon give (van Putten 2015a)

$$\Lambda = (1 - q)H^2. \tag{5}$$

Discrepant dispersion relations of its temperature and holographic image modes are found to exhibit non-Newtonian behavior in weak gravity, asymptotically described by Milgrom's law parameterized by $(H, q)$. In the de Sitter limit $(q = -1)$, Milgrom's parameter reduces to (van Putten 2016)

$$a_0 = \frac{H}{\sqrt{2}\,\pi}. \tag{6}$$

In this paper, (5) is shown to have a holographic origin in intrinsic surface gravity of the cosmological horizon (with no recourse to temperature) and the onset to weak gravity is found to be a sharp transition. The latter arises from a thermodynamic potential

$$U = mc^2 \tag{7}$$

of inertia $m$ in Rindler spacetime, which is perturbed to $m$ below the Newtonian value $m_0$ by causality as Rindler and cosmological horizon surfaces collude. For our three-flat FRW cosmology, the results are confronted with recent high-resolution data on galaxy rotation curves (Lelli et al. 2016). An outlook on galactic dynamics as a novel probe of (5) is included for future surveys of low-redshift galaxies.

In Section 2, we highlight weak gravity in departure of Newtonian and strong gravitation described by general relativity. Section 3 illustrates dimensional reduction by scaling, pointing to holography of horizon surfaces. In Section 4, inertia is expressed by a thermodynamic potential associated with Rindler horizons in Minkowski spacetime. Section 5 introduces collusion of Rindler horizons with the cosmological horizon, giving rise to reduced inertia in weak gravity. A holographic derivation of dynamical dark energy from intrinic surface gravity of the cosmological horizon in general FRW cosmologies is given in Section 6, parameterized by $(H, q)$. Astrophysical consequences are discussed in Section 7, highlighted by a transition to reduced inertia in the case of small accelerations, confronted with recent data of galaxy rotation curves. Galactic dynamics hereby can be used to probe cosmological parameters, including a test of dynamical dark energy (Section 8). We summarize our findings with an upper bound on the mass of the putative dark matter particle (Section 9).

## 2. Limits of Gravitation

The Hamiltonian of a test particle in polar coordinates $(r, \varphi)$ provides a convenient setting to classify weak, normal, and strong gravity. Following the Möbius transformation $u = 1/r$ with $u = u(\varphi)$, and exploiting conservation of specific angular momentum $j = r^2\dot{\varphi}$, the Hamiltonian satisfies

$$H = \frac{1}{2}j^2u'^2 + U \tag{8}$$

with Newton's potential

$$U_N = \frac{1}{2}(u - u_0)^2 + U_0, \tag{9}$$

where $u_0 = GM/j^2$ and $U_0$ is a constant. Here, we suppress explicit mention of test particle inertia, equal to its rest mass $m_0$.

Bound motions $(H < 0)$ have $u(\varphi)$ harmonic in $\varphi$, $u'' + u = u_0$ with the solutions of Keplerian orbits $u = u_0(1 + e\cos\varphi)$ $(e < 1)$. Newton's theory of gravitation gives a satisfactory explanation of planetary motions in the solar system, except for Mercury. Historically of great significance, the latter shows a non-Newtonian, geodetic precession described by (8) with Einstein's potential (Figure 1)

$$U_E = U_N - R_g u^3 \tag{10}$$

parameterized by the gravitational radius

$$R_g = \frac{GM}{c^2} = 1.5 \times 10^5 \left(\frac{M}{M_\odot}\right) \mathrm{cm} \tag{11}$$

of a mass $M$, normalized to a solar mass $M_\odot = 2 \times 10^{33}$ g. Thus, the Schwarzschild radius $R_S = 2R_g$ provides a scale, separating Newtonian gravity $(r \gg R_g)$ from strong gravity $(r \sim R_g)$.

On a cosmological background, the Hubble radius $R_H$ of the cosmological horizon appears as an additional scale in the elliptic part of general relativity, that governs gravitational attraction. We shall refer to weak gravity the limit at which the presence of the cosmological horizon is important (Figure 1).

## 3. Weak Gravity by Dimensional Reduction

By dimensional analysis, the unit of luminosity $L_0$ introduces a pressure

$$p_0 = -\frac{L_0}{cA_H} \tag{12}$$

on the cosmological horizon with area $A_H = 4\pi R_H^2$. In ΛCDM, the three-flat de Sitter limit described by a deceleration parameter $q = -1$ has a Lorentz invariant cosmological horizon. As such, $p_0$ has an associated energy density $\rho_0 = -p_0$, whereby (van Putten 2015a)

$$\Omega_\Lambda = \frac{\rho_0}{\rho_c} = \frac{2}{3}, \tag{13}$$

close to today's state of the universe; see also (Easson et al. 2011).

As mentioned, upon conversion to geometrical units, (13) represents a surface energy density $[\sqrt{\Lambda}]$. Equating the total surface energy $A\sqrt{\Lambda} \simeq A\sqrt{2}H$ on a sphere of area $A = 4\pi r^2$ with the mass $M$ of a galaxy enclosed within obtains a transition radius

$$r_t \sim \sqrt{R_g R_H}, \tag{14}$$

where $R_g = GM/c^2$ according to (11). Applied to a galaxy of mass $M = M_{11}10^{11}M_\odot$, $r_t$ defines a characteristic radius on the order of a kiloparsec beyond. This corresponds to the scale at which galaxy rotation curves show non-Newtonian behavior on the basis of baryonic matter content. By volume, most of the universe is hereby governed by weak gravity.

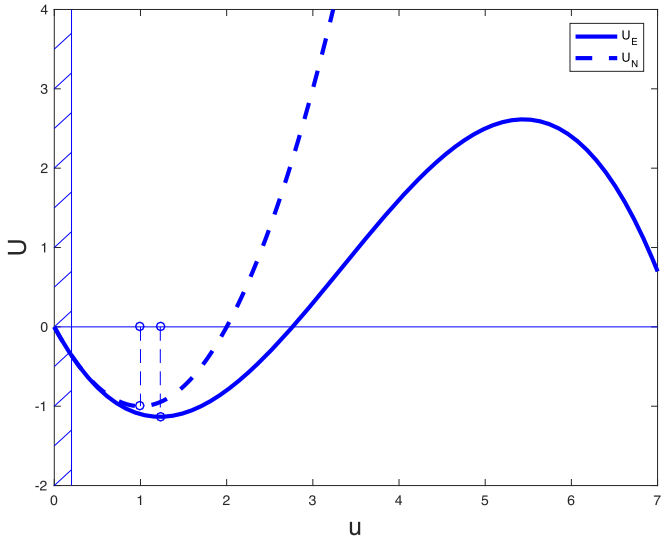


**Figure 1.** Shown are the Newton and Einstein potentials $U_N$ and, respectively, $U_E$ in the Hamiltonian of orbital motion (8). In $U_E$, symmetry about its local minimum is lost. The vertical dashed lines refer to a shift in radius of circular motion due to the cubic nonlinearity in $U_E$. The shaded strip about $u = 0$ refers to cosmological distances, representative of weak gravity associated with the Hubble radius.

In what follows, we elaborate on the above in more detail by thermodynamic properties and causality of horizon surfaces, of Rindler and the cosmological horizons.

## 4. Thermodynamic Origin of Inertia

Locally, the vacuum is Minkowskian described by Lorentz invariant light cones $ds = 0$ at each point of spacetime. In a Newtonian description, stars in galaxies are mutually interacting by gravitational forces that put them on non-inertial trajectories in flat Minkowski spacetime at zero temperature vacuum. (These trajectories become geodesic in curved spacetime described by general relativity.) Observers along such trajectories see things differently.

At acceleration $\alpha$, the world-line of a Rindler observer (Birrell & Davies 1982) has a time-dependent rapidity $\lambda(\tau) = \alpha\tau$ as a function of eigentime $\tau$. In a Minkowski diagram, the trajectory of $x^b(\tau) = \xi(\sinh\lambda, \cosh\lambda)$ appears curved with $x^b(0) = (0, \xi)$ at a constant distance of $\xi = c^2/\alpha$ according to the line-element $ds^2 = -dt^2 + dx^2$ of $1 + 1$ Minkowski spacetime $(t, x)$. $\mathcal{O}$ hereby assumes a constant distance $\xi$ to its Rindler event horizon $h$, a light cone with vertex at the origin (Figure 2) satisfying

$$\alpha\xi = c^2. \tag{15}$$

Thus, $\mathcal{O}$'s field of view is limited to a wedge Minkowski spacetime. In this wedge, $\mathcal{O}$ shares only a finite interval $\Delta\tau = \pi\xi/c$ of its eigentime $\tau$ with inertial observers in Minkowski spacetime.

According to (15), $\mathcal{O}$ is trailed by $h$ at a distance $\xi$ inversely proportional to $a$.

In unitary holography, a particle of mass $m_0$ at a distance $\xi$ is imaged by information (van Putten 2015b)

$$I = 2\pi\Delta\varphi \tag{16}$$

on two-dimensional screens, that cover an Einstein area $A_E = 8\pi\Delta\varphi l_p^2$ in terms of the Compton phase $\Delta\varphi = k\xi$ defined by the wave number $k = m_0 c/\hbar$ and the Planck-sized elements of area $l_p^2 = G\hbar/c^3$, where $\hbar$ denotes the Planck constant. Holography is hereby realized by imposing unitarity $P_+ + P_- = 1$ on the transition probabilities for $m$ to be inside $(P_+)$ or outside $(P_-)$ a screen of radius $\xi$ about $m_0$.

$I$ in (16) follows from unitarity as an exact relation with no round-off. Exact arithmetic on exponentially small probabilities in macroscopic configurations hereby entails a large, discrete number of units of information (e.g., bits), proportional to distances measured in the Compton phase. For position information of mass, this comprises an area of $(1/4)A_E$. The factor $2\pi$ in (16) is specific to spherical screens. Minimal and maximal screens correspond to, respectively, event horizons of black holes and the cosmological horizon, in which case $I$ reduces to entropy. Furthermore, the trival propagator of vacuum fluctuations circumvents the coupling of zero-point energies to spacetime curvature.

In Minkowski spacetime, Rindler observers detect the Unruh temperature (Unruh 1976)

$$k_B T_U = \frac{\hbar\alpha}{2\pi c} \tag{17}$$

associated with the surface gravity of $h$. This is a most remarkable prediction on black-body radiation emerging from the vacuum, on equal footing to warm bodies of baryonic matter. By its thermal spectrum, $h$ is attributed Planck-sized degrees of freedom to account for an entropy very similar to that associated with black-hole event horizons.

To highlight its basic premises, we recall that (17) derives from a Bogoliubov map, by ray tracing between radiative Hilbert spaces $\mathcal{H}_X$ and $\mathcal{H}_Y$ in the past and, respectively, future (Birrell & Davies 1982), here shown in Figure 2 with null surface elements $X$ and $Y$ as indicated. A choice of uniform distribution of phase on $Y$ defines a given positive frequency state of $\mathcal{H}_Y$ relative to $|0\rangle$. The ray tracing map thus introduces a Fourier transform on $X$ of a logarithmic distribution of phase $\phi(x) = \alpha\ln x$ over $X = (0, \infty)$, giving rise to a thermal spectrum $|\beta|^2 = (e^{2\pi\alpha} - 1)^{-1}$ (Birrell & Davies 1982).

In this process, a Rindler observer, according to its eigentime, detects a wave front with exponential divergence in frequency into the future. Starting from the true vacuum state of $X$, the inverse of our map gives a thermal distribution of positive energy photon number (per unit time per unit frequency) $|\beta|^2$ out to the future through $Y$ (Birrell & Davies 1982).

At a distance $\xi$ to $h$, changes in $\xi$ introduce a corresponding change in entropy $dS = -k_B dI$ at $T_U$ of $\alpha$ on $h$, and $T_U = k_B^{-1}(\partial S/\partial m_0 c^2)^{-1} \equiv a\hbar(2\pi c)$ is also a thermodynamic temperature. Inertia of Rindler observers hereby satisfies

$$F = -T_U\frac{dS}{d\xi} = \left(\frac{\hbar\alpha}{2\pi c}\right)\left(2\pi\frac{mc}{\hbar}\right) = m_0\alpha \tag{18}$$

with associated potential energy relative to $h$ equal to its rest-mass energy,

$$U = \int_h^{\mathcal{O}} F ds = F\xi = m_0 c^2, \tag{19}$$

by virtue of $\alpha$ being constant along $\xi$.

In (19), inertia $m = m_0$ originates in the thermodynamic potential $U$ associated with the Rindler horizon $h$. Causality imposed on integration between $\mathcal{O}$ and $h$ implies that $m$ drops

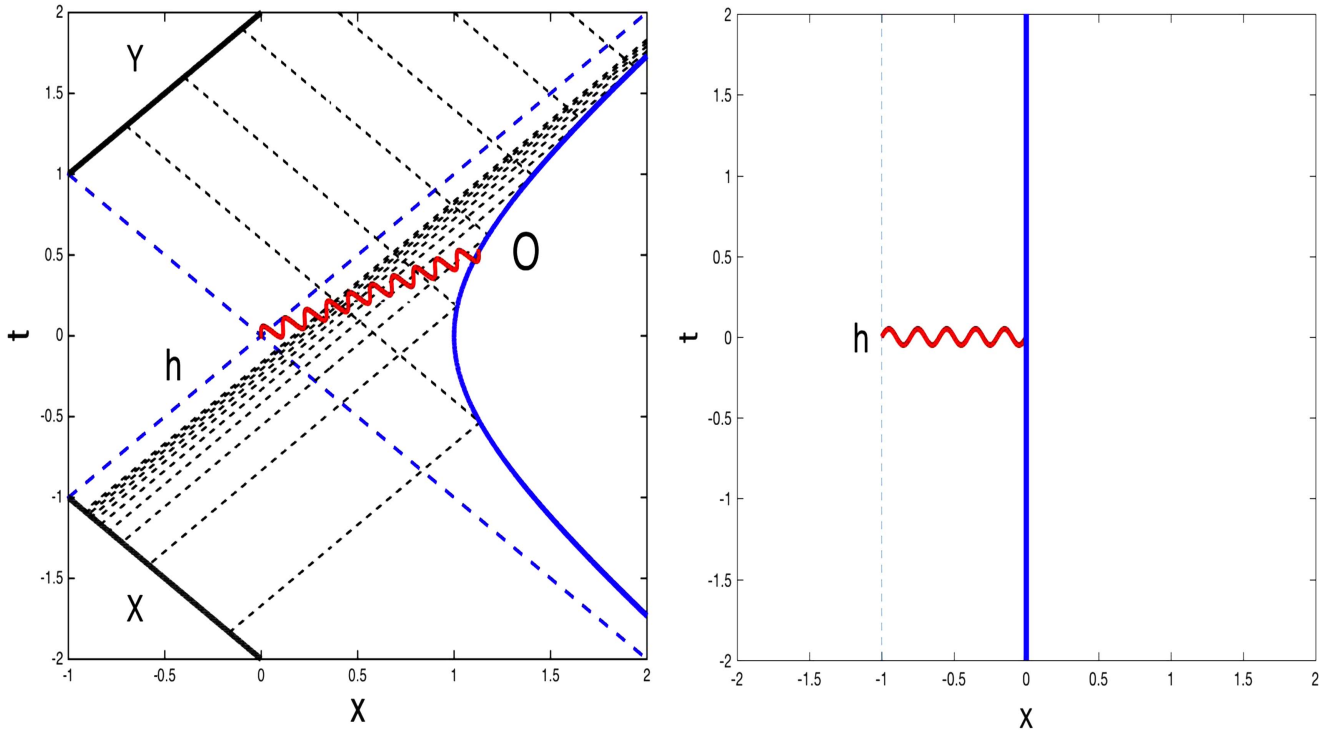


**Figure 2.** (Left panel) A light cone in Minkowski space forms a horizon surface of a Rindler observer $\mathcal{O}$ moving at constant acceleration $a$. It assumes a finite temperature of that derived from a map of phase uniform on a null surface element $Y$ in the future into a logarithmic distribution on a null surface element $X$ in the past (adapted from Birell & Davis 1982). Vacuum in the past hereby has a corresponding non-zero state in the future, that appears to $\mathcal{O}$ at the Unruh temperature (17). (Right panel) A Rindler observer $\mathcal{O}$ is trailed by an event horizon $h$ at constant distance $\xi$, whose inertia can be attributed to a thermodynamic potential associated with $h$.

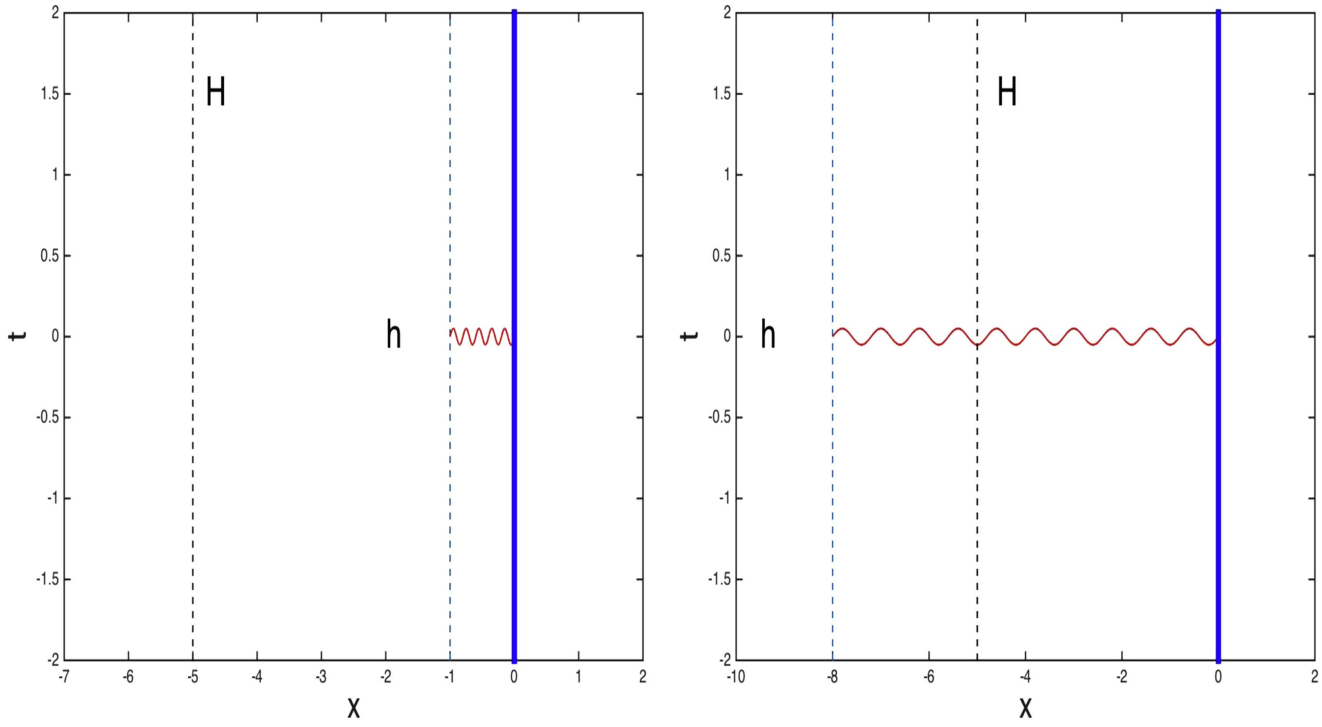


**Figure 3.** (Left panel) A Rindler observer $\mathcal{O}$ is trailed by an event horizon $h$ at constant distance $\xi$, whose inertia can be attributed to a thermodynamic potential associated with $h$. Normal (left panel) and weak gravity limits (right panel) are defined by $\xi$ relative to the distance $R_H$ to the cosmological horizon $H$ as seen by inertial observers. The latter signals a perturbation of $\mathcal{O}$ inertia below its Newtonian value.

below $m_0$ in (7), whenever $h$ falls beyond the cosmological horizon $H$.

## 5. Colluding Rindler and Cosmological Horizons

On cosmological scales, the vacuum has a small but finite Gibbons–Hawking temperature (Gibbons & Hawking 1977)

$$T_{dS} = \frac{cH_0}{2\pi k_B} \simeq 3 \times 10^{-30}\,\mathrm{K} \tag{20}$$

associated with the cosmological horizon at $R_H = c/H_0$ in the limit of Lorentz invariant de Sitter space, where $k_B$ denotes the Boltzmann constant.

A collusion of the Rindler and cosmological horizon (Figure 3) occurs when $\xi = c^2/\alpha$ satisfies

$$\xi = R_H. \tag{21}$$

In dynamics of spiral galaxies of mass $M = M_{11}10^{11}M_0$ with gravitational radius $R_g$ according to (11) by a Newtonian gravitational attraction $a_N = GM/r^2$, $a_N \sim a_H = c^2/R_H$, we thus arrive at a transition radius (van Putten 2016)

$$r_t = \sqrt{R_H R_g} = 4.7\, M_{11}^{\frac{1}{2}}\,\mathrm{kpc} \tag{22}$$

beyond which we reach weak gravity with

$$\xi > R_H. \tag{23}$$

In the following, we pursue the weak gravity regime (22)–(23). According to Section 4, rest mass equals the potential energy in the gravitational field associated with the Rindler horizon in Minkowski space, whereby inertia and total mass energy are identical. This will be perturbed in weak gravity in FRW cosmologies, as the Rindler horizon $h$ drops beyond $H$.

## 6. Holographic Dynamical Dark Energy

In FRW cosmologies, cosmological horizons are trapped surfaces defined in hypersurfaces of constant cosmic time $t$. Given a unit normal $s^i$ and an extrensic curvature $K_{ij} = \nabla_i s_j$, they satisfy $\nabla_i s^i + s_i s_i K^{ij} - K = 0$ (Brewin 1988; York 1989; Wald & Iyer 1991; Cook & Abrahams 1992; Cook 2000; Thornburg 2007). In three-flat FRW cosmologies with Hubble parameter $H$, this reduces to $\nabla_i s^i = 2H$, i.e., $R_H = c/H$ as stated before. A covariant derivation of surface gravity obtains from geodesic deviation between a pair of generators in four-dimensional spacetime $(t, r, \theta, \varphi)$ centered about an inertial observer. A tangent $k^b$ to such a generator is null, $k^t k^t - a^2 r^2 k^\theta k^\theta = 0$. A space-like separation $l$ in $\Sigma_t$ between such null-generators, initially along the unit vector $m^c = a^{-1}r^{-1}$ $(0, 0, 1, 0)$ experiences a change in length with tip-to-tip acceleration, given by the equation of geodesic deviation along $m^c$. With cosmic time $t$ as an affine parameter, $k^t = 1$, the acceleration $\alpha^b$ of one tip satisfies

$$\alpha^b = -\frac{1}{2}R_{aec}{}^b k^a k^c m^e = -a\frac{1}{2}(1-q)H, \tag{24}$$

where $R_{abcd}$ denotes the Riemann tensor of the FRW line-element (Pirani 1957). In magnitude, $\alpha = \sqrt{\alpha^c \alpha_c}$ satisfies the intrinsic surface gravity

$$a_H = \frac{1}{2}(1-q)H. \tag{25}$$

We may infer from (25) a thermodynamic temperature $T_H = \hbar a_H/2\pi c$ (Cai & Kim 2005; van Putten 2015a), where $\hbar$ is Planck's constant.

Illustrative is an application to black-hole event horizons, upon considering a null-tangent $k^b = (k^t, k^\theta)$ of the event horizon of a Schwarzschild black hole with mass $M$. It has the intrinsic surface gravity

$$a_H = \frac{GM}{r_H^2} = \frac{c^4}{4GM} \tag{26}$$

equal to the extrinsic surface gravity

$$a_H' \equiv -\lim_{r\to r_H}\frac{dA}{ds} \tag{27}$$

in the Schwarzschild line-element with $ds = dr/A$, and redshift factor $A(r) = \sqrt{1-2R_g/r}$, $R_g = GM/c^2$. This surface gravity conforms to Hawking's thermodynamic temperature (Hawking 1975) $T_H = \hbar a_H(2\pi)$ akin to (7): a test particle of rest mass $m = \delta M \ll M$ taken from $H$ to infinity is associated with entropic work $W = T_H \delta S = mT_H(\partial S_H/\partial Mc^2) = mc^2$, based on the Bekenstein–Hawking entropy $S_H = (1/4)k_B A_H/l_p^2$ (Bekenstein 1973; Hawking 1975), where $l_p = \sqrt{G\hbar/c^3}$ denotes the Planck length. In the Schwarzschild line-element of black holes, the same result obtains from the line-integral of force $F = m_0 GM/r^2$ over distance $s$ from $R_H = 2R_g$ to infinfity, i.e., $U(r) = \int_{R_H}^r F ds = \sqrt{1-2M/r}\, m_0 c^2$. This recovers

$$U = \int_{R_H}^\infty F ds = m_0 c^2 \tag{28}$$

as the gravitational binding energy of a mass element $m_0$ in the black hole. Hidden behind the event horizon, the source of the gravitational field is again unseen (Penrose 1965).

In a Cartesian coordinate system, $dy = rd\theta$ at $r = R_H$, the geodesic deviation Equation (24) gives $\ddot{l}\delta_{3d} = -lR_{abcd}k^a k^c m^b = -a(1-q)H^2 l$ for the acceleration of separation $l$ parallelly transported between two null-generators of a horizon null surface. Upon taking the norm of $\delta_{3d}$, this defines a harmonic oscillation

$$\ddot{u} + \omega_0^2 u = 0,\ \omega_0 = \sqrt{1-q}\,H_0 \tag{29}$$

that, in a holographic approach, extends to a wave equation in spacetime within

$$\Box u + \Lambda u = 0,\ \omega = \sqrt{c^2k^2 + \hbar^2\Lambda} \tag{30}$$

with $\Lambda$ given by (5). The wave Equation (30) will be recognized to describe electromagnetic and linearized gravitational waves in de Sitter space, considered in a Lorenz gauge on the U(1) and, respectively, SO(3, 1) connection (Wald 1984; van Putten & Eardley 1996), by coupling to the Ricci tensor $R_{ab} = c^{-2}\Lambda g_{ab}$. Importantly, (30) reveals a dispersion at low energies.

With (5), three-flat universes with densities of dark and baryonic matter $\Omega_M$ and a dark energy $\Omega_\Lambda$

$$\Omega_M + \Omega_\Lambda = 1 \tag{31}$$

are described by modified FRW equations, satisfying (van Putten 2015a)

$$\Omega_M = \frac{1}{3}(2+q),\ \Omega_\Lambda = \frac{1}{3}(1-q). \tag{32}$$

Thus, three-flat de Sitter cosmologies ($q=-1$) satisfy $\Omega_M = 1/3$ and $\Omega_\Lambda = 2/3$, in contrast to $\Omega_M = 0$ and $\Omega_\Lambda = 1$ in ΛCDM.

## 7. Reduced Inertia in Galactic Dynamics

In weak gravity (23), (7) is reduced by integration limited to $R_H$, whereby $mc^2 \propto (R_H/\xi)m_0c^2$. As a holographic condition at equipartition, we impose equality in the number of radial bulk modes and two-dimensional screen modes,

$$\frac{mc^2}{\frac{1}{2}\sqrt{\hbar^2\Lambda + c^2p^2}} = \frac{(R_H/\xi)m_0c^2}{k_B\sqrt{T_H^2 + c^2p^2}}, \tag{33}$$

where $p$ refers to a momentum coupling between screen and bulk modes, and $T_H$ is the cosmological horizon temperature associated with the above mentioned intrinsic surface gravity,

$$T_H = \left(\frac{1-q}{2}\right)T_{dS}. \tag{34}$$

With $R_H/\xi = \alpha/a_{dS}$, it follows that $m = m_0\alpha/(2Ba_{dS})$ with

$$B(p) = \frac{k_B\sqrt{T_H^2 + c^2p^2}}{\sqrt{\hbar^2\Lambda + c^2p^2}}. \tag{35}$$

Given a gravitational attraction $F_N = GMm_0/r^2 \equiv a_N m_0$ by a baryonic mass $M$, we thus arrive at an acceleration

$$\alpha = \sqrt{2Ba_{dS}a_N}. \tag{36}$$

At very low momenta,

$$\xi \gg R_H \tag{37}$$

$B \simeq B(0) = k_BT_H/\hbar\sqrt{\Lambda} = \beta_0\sqrt{(1-q)/2}$, and

$$\beta_0 = \frac{1}{2\sqrt{2}\pi} \tag{38}$$

in (36) captures Milgrom's emperical asymptotic relation

$$\alpha = \sqrt{a_0a_N} \tag{39}$$

of an inverse distance law of gravity. Here $a_0$ is Milgrom's constant $a_0$ with $a_0 = 2B(0)a_H$ in (36), i.e., (van Putten 2016, corrected by a factor of two)

$$a_0 = \frac{cH}{2\pi}\sqrt{1-q}. \tag{40}$$

Presently, we have

$$a_0|_{z=0} = 1.32\,h_0\left(\frac{1-q}{1.5}\right)^{\frac{1}{2}}\ \text{Å s}^{-2}. \tag{41}$$

where $h_0$ refers to the present Hubble parameter normalized to $H_0 \simeq 70\ \text{km s}^{-1}\ \text{Mpc}^{-1}$.

The weak gravity limit (36)–(37) is well known for its description of galaxy rotation curves. A continuous transition to the normal, Newtonian gravity regime $\xi \geqslant R_H$ may be expressed by a running Milgrom parameter $a_0$, satisfying $a_0 = a_N$ at $\xi = R_H$. This has led to various phenomenological interpolation functions as a function of acceleration $\alpha$ (Famae & McGaugh 2012).

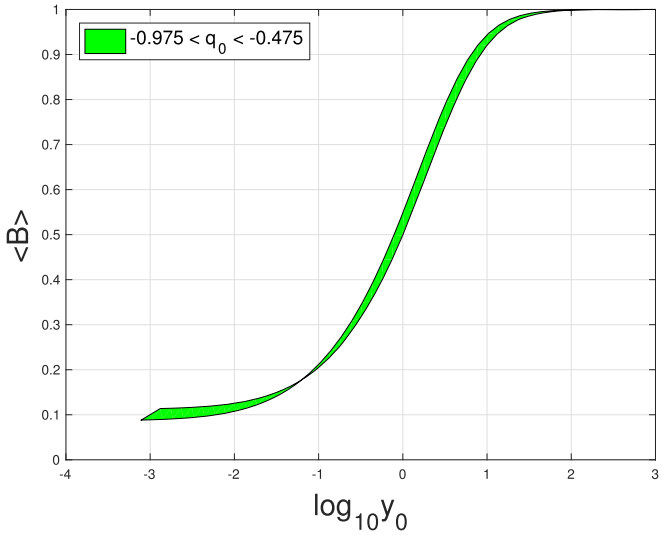


**Figure 4.** Thermal average $\langle B\rangle$ as a function of normalized acceleration $y_0 = T/T_{dS}$ over a range of deceleration parameters $q$. The domain of weak gravity is $y_0 \leqslant 1$.

The transition region between the onset (21) and $\xi \gg R_H$ is described by a momentum dependent coefficient $B = B(p)$. In associating $p = |\boldsymbol{p}|$ with an isotropic distribution of vacuum fluctuations, we propose the thermal average

$$\langle B\rangle_T = \frac{1}{W}\int_0^\infty B(p)e^{-\frac{E}{k_BT}}(4\pi p^2)dp, \tag{42}$$

$W = \int_0^\infty e^{-\frac{E}{k_BT}}(4\pi p^2)dp$, with $E = \sqrt{\hbar^2\Lambda + c^2p^2} - \hbar\sqrt{\Lambda}$. For numerical evaluation, we express (42) as

$$\langle B\rangle_y = \frac{1}{W}\int_0^\infty f(x)e^{-e/y}x^2dx, \tag{43}$$

$W = \int_0^\infty e^{-e/y}x^2dx$, $f(x) = \sqrt{1+x^2}/\sqrt{A+x^2}$, $e = \sqrt{A+x^2} - A^{1/2}$, $A = 16\pi^2/(1-q)$, $y = T/T_H$ with (34),

$$y = y_0\left(\frac{1-q}{2}\right)^{-1},\quad y_0 = \frac{T}{T_{dS}}. \tag{44}$$

The thermal average $\langle B\rangle_y$ has the property that $\langle B\rangle_1 \simeq 1/2$, shown in Figure 4.

To be precise, $\langle B\rangle_1 = 0.4691$ for $q = -0.5$ and $\langle B\rangle_1 = 0.4995$ for $q = -1$, effectively ensuring continuity $\alpha \simeq a_{dS}$ in transition to weak gravity (23), while $\langle B\rangle_y \to B(0)$ as $y \to 0$. On this basis, we apply (43) to weak gravity with $y_0 = a_N/a_{dS}$.

Figure 5 shows a confrontation of inertia $m/m_0 = a_N/\alpha$ in spiral galaxies at essentially zero redshift, where $\alpha$ is the observed acceleration $a$ and $a_N$ is the Newtonian acceleration $a_N$ based on baryonic matter.

The data in Figure 5 show a sharp onset at $a_N = a_{dS}$ to weak gravity at the causal crossing (21). It represents a cutoff in the thermodynamic potential of inertia. As such, there is no continuation of the green curve to the right of (21). With (42), we arrive at a complete transition to (36), i.e., Milgrom's law in the asymptotic regime for $a_N \ll a_{dS}$ in (23).

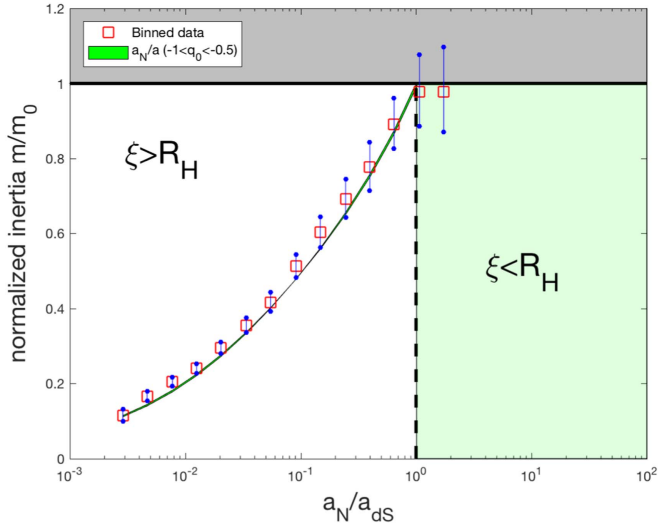


**Figure 5.** Newtonian accelerations $a_N = a_{dS}$ define an onset to weak gravity at (21) as Rindler and cosmological horizon collude. For $a_N < a_{dS}$, $\alpha > a_N$ as inertia $m$ drops below the Newtonian value $m_0$. This onset is sharp as manifest in galaxy rotation curves, here plotted as $m/m_0$ as a function of normalized acceleration $a_N/a_{dS}$ based on baryonic matter content. Shown are binned data accompanied by $3\sigma$ uncertainties. The curved green band is the theoretical curve covering $-1 < q_0 < -0.5$ with $H_0 = 71\,\mathrm{km\,s^{-1}\,Mpc^{-1}}$. (Data from Lelli et al. 2016).

## 8. Probing Deceleration and the Mass of Dark Matter

Measurements of Hubble parameter $H = H(z)$ and the deceleration parameter $q(z)$ provide a powerful probe of cosmic expansion that may be obtained from local surveys independent of cosmological models.

Inverting (40) gives the measurement of the deceleration parameter,

$$q(z) = 1 - \left(\frac{2\pi a_0(z)}{cH(z)}\right)^2. \tag{45}$$

For $q_0 = q(0)$, we encounter uncertainties in $a_0(0)$ and $H_0 = H(0)$. A best fit to the data of Figure 5 based on least square errors shows

$$q_0 \simeq -0.7 + 0.2(H_0' - 71) \tag{46}$$

as a function of $H_0 = H_0'\,\mathrm{km\,s^{-1}\,Mpc^{-1}}$ and based on the 12 data points in the transition region $a_N < a_H$ shown in Figure 5. The correlation (46) takes into account a scaling of galaxy rotation velocity data $V_c^2/M$ with $H^{-1}$ for galaxies satisfying a constant mass-to-light ratio.

Redshift dependence in (40) may be probed by future galaxy surveys, enabling a probe of our dynamical dark energy (5) as a key manifestation of cosmological holography. In particular, this may determine $Q(z) = dq(z)/dz$,

$$Q(z) = 2(1-q)\left(H^{-1}\frac{dH}{dz} - a_0^{-1}\frac{da_0(z)}{dz}\right) \tag{47}$$

with $H^{-1}dH/dz = (1+q)/(1+z)$. The measurement of $Q_0 = Q(0)$ in (47) enables a direct test of dynamical versus static dark energy, i.e., (5) versus ΛCDM, with (van Putten 2016)

$$Q_{0,\mathrm{dyn}} > 2.5, \quad Q_{0,\mathrm{stat}} < 1. \tag{48}$$

Furthermore, $A_0 = A(0)$, $A(z) = a_0^{-1}da_0(z)/dz$, is similarly distinct: $A_{0,dyn} \simeq -0.5$ and $A_{0,stat} > 0$.

## 9. Conclusions and Outlook

Here, we consider a confrontation of the equivalence principle with $a_{dS}$ that by causality appears as a new scale in weak gravity. We have given a thermodynamical origin of inertia in the potential (7) and a holographic origin of dynamical dark energy (5) in intrinsic curvature of the cosmological horizon $H$. In recent high-resolution data of Lelli et al. (2016), we point out a transition to weak gravity that effectively coincides with $a_N = a_{dS}$. This onset remained elusive in earlier data (Famae & McGaugh 2012).

These issues are connected by causality. The potential (7) is perturbed whenever the Rindler horizon $h$ falls behind $H$, taking $m$ below its Newtonian value $m_0$ whenever $a_N < a_{dS}$. The asymptotic regime $a_N \ll a_{dS}$ corresponds to the baryonic Tully–Fisher law, i.e., Milgrom's law (39) parameterized by $a_0$ in (40) based on discrepant dispersion relations on $H$ and its three-dimensional image within. By (5), $a_0$ is expressed in terms of the canonical FRW parameters $(H, q)$ and hence is no longer a phenomenological parameter.

The transition about $a_N = a_{dS}$ with $m < m_0$ to the left and $m = m_0$ to the right is sharp in $C^0$. The first is evident by a finite slope supported by tight binned data in Figure 5. At the $3\sigma$ uncertainties shown, the second is tentative, and may be confirmed with improved resolution obtained from future galaxy rotation surveys. Based on the well-resolved data to the left, we note that any smooth (continuously differentiable) turnover incurs an overshoot of $m/m_0 > 1$ to the right of (21), which would seem odd.

The sharp transition at $a_N = a_{dS}$ in Figure 5 appears to be an entirely new challenge in explaining galaxy rotation curves by extended cold or warm dark matter distributions. Our theory obviates the need for dark matter on these scales. Nevertheless (32), (46) and the general consensus $-1 < q < -0.5$ suggest the need for a cosmological distribution of dark matter, e.g., down to galaxy clusters (van Putten 2015a). If so, dark matter clustering is limited to scales larger than individual galaxies (e.g., Vikram et al. 2015). This puts a bound on the mass of the putative dark matter particle,

$$m_D \leqslant 10^{-30}\,\mathrm{eV}, \tag{49}$$

somewhat higher than the mass scale $\hbar\sqrt{\Lambda} \simeq 2\sqrt{2}\,\pi k_B T_{dS} = 2 \times 10^{-33}$ eV associated with the de Sitter temperature of the cosmological horizon. This mass scale (49) may, for instance, be attributed to low temperature pairing of bosons (e.g., van Putten 2010).

In our approach, we apply Rindler horizons defined in Minkowski spacetime to cosmology in standard line-elements that are three-flat. The same does not necessarily carry over to freefall on Earth, whose gravitational field is conformally three-flat (in isotropic coordinates, ignoring frame-dragging). Freefall at the edge of a galaxy and on Earth is conceivably inequivalent, and laboratory experiments on freefall perturbations on the scale of $a_{dS}$ need not reveal reduced inertia such as shown in Figure 5. It may be of interest to address this experimentally, to determine the outcome of such minute perturbations (vertical versus horizontal), on Earth and in space. Realization of $\alpha > a_N$ promises novel details on the limits of Newtonian inertia, gravitation and the equivalence principle

The explicit sensitivity of galaxy rotation curves to the cosmological background, by (40) and its inverse (45), may be used to probe $Q_0$ by (47), to confirm or falsify dynamical dark energy or LambdaCDM according to (48). This may be

pursued by galaxy rotation surveys that extend into the low-redshift regime, beyond the present data about $z \simeq 0$.

The author thanks the anonymous referee for constructive comments and a detailed reading of the manuscript. This report is supported in part by the Korean National Research Foundation under Grants 2015R1D1A1A01059793 and 2016R1A5A1013277.

## References

Ade, P. A. R., Aghanim, N., Alves, M. I. R., et al. 2014, A&A, 571, A1
Bekenstein, J. 2009, NuPhA, 826, 555
Bekenstein, J. D. 1973, PhRvD, 7, 2333
Bekenstein, J. D. 1981, PhRvD, 23, 287
Birrell, N. D., & Davies, P. C. W. 1982, Quantum Fields in Curved Space (Cambridge: Cambridge Univ. Press)
Brewin, L. 1988, PhRvD, 38, 3020
Cai, R.-G., & Kim, S. P. 2005, JHEP, 2, 50
Cook, G. B. 2000, LRR, 3, 5
Cook, G. B., & Abrahams, A. M. 1992, PhRvD, 46, 702
Easson, D. A., Frampton, P. H., & Smoot, G. F. 2011, PhLB, 696, 273
Famaey, B., & McGaugh, S. S. 2012, Living Reviews, 15, 10
Gibbons, G. W., & Hawking, S. W. 1977, PhRvD, 15, 2738
Hawking, S. 1975, CMaPh, 43, 199
Lelli, F., McGaugh, S. S., Schombert, J. M., & Pawlowski, M. S. 2016, arXiv:1610.08981v1
LIGO-Virgo Collaboration 2016, PhRvL, 116, 241102
McGaugh, S. S. 2005, ApJ, 632, 859
McGaugh, S. S. 2011, PhRvL, 106, 121303
McGaugh, S. S. 2012, AJ, 143, 40
McGaugh, S. S., & Lelli, F. 2016, PhRvL, 117, 201101
McGaugh, S. S., & Schombert, J. M. 2015, ApJ, 802, 18
Milgrom, M. 1983, ApJ, 270, 365
Penrose, R. 1965, PhRvL, 14, 57
Perlmutter, S., Aldering, G., Goldhaber, G., et al. 1999, ApJ, 517, 565
Pirani, F. A. E. 1957, PhRv, 105, 1089
Riess, A. G., Macri, L. M., Hoffmann, S. L., et al. 2016, ApJ, 826, 56
Susskind, L. 1995, JMP, 36, 6377
t Hooft, G. 1993, arXiv:gr-qc/9310026
Thornburg, J. 2007, LRR, 10, 7
Unruh, W. G. 1976, PhRvD, 14, 870
van Putten 2015a, MNRAS, 450, L48
van Putten, M. H. P. M. 2010, PhLA, 374, 3346
van Putten, M. H. P. M. 2015a, MNRAS, 405, L48
van Putten, M. H. P. M. 2015b, IJMP, 24, 1550024
van Putten, M. H. P. M. 2016, ApJ, 824, 43
van Putten, M. H. P. M., & Eardley, D. M. 1996, PhRvD., 53, 3056
Vikram, V., Chang, C., Jain, B., et al. 2015, PhRvD, 92, 2006
Wald, R. M. 1984, General Relativity (Chicago, IL: Univ. Chicago Press)
Wald, R. M., & Iyer, V. 1991, PhRvD, 44, R3719
York, J. W. 1989, in Frontiers in Numerical Relativity, ed. C. R. Evans, L. S. Finn, & D. W. Hobill (Cambridge: Cambridge Univ. Press)